6

Speciation and Solubility Modeling

6.1 Introduction

The application of speciation–solubility in geochemistry goes back to Garrels and Thompson (1962), who calculated the aqueous speciation in seawater and saturation states with respect to mineral solubilities. Since then, this subject has been treated extensively, and hundreds of codes are available for this kind of calculation. In principle, the concentration and activity coefficients of all aqueous species can be calculated if there are the same number of equations as unknowns. Given an equilibrium constant for each complex, plus an analysis giving the total quantity of each basis species, this is usually possible.

Speciation–solubility calculations provide a "snapshot" of the (assumed) equilibrium state of a dynamic system. That is, the chemical composition of a water sample is obtained, and assuming that the chemical species in the solution are at mutual equilibrium (*homogeneous equilibrium*), the concentrations and activities of the various ionic and molecular species present are calculated. Then, using these calculated quantities, the saturation states (i.e., whether superstaurated or undersaturated) of all possible pure solids and gases are calculated, as described in Chapter 3. Here, "all possible" refers to the fact that the range of solids and gases that can be calculated to exist in the system is limited by the chemical components in the water analysis. One cannot infer anything about the saturation state of calcite (or any other mineral containing calcium) if the water has not been analyzed for calcium.

The interpretation of calculated mineral Saturation Indices is not simple, and is discussed in §6.2.7.

https://doi.org/10.1017/CBO9780511606274.007 Published online by Cambridge University Press

Figure 6.1. Overview of the Bear Creek Uranium tailings site, looking toward the south. The white buildings on the left, now demolished, indicate where the uranium mill operated from the 1970s to the mid-1980s. Spent acids and tailings slurries were piped to tailings ponds behind the tailings dams. This site has now been reclaimed.

6.2 A Uranium Mill Tailings Impoundment

6.2.1 The Site

The Bear Creek Uranium site is located in the southern part of the Powder River basin in Wyoming, and presents an example of uranium mill tailings and acid mine drainage (AMD) problems typically associated with mine tailings. A uranium mill operated from the 1970s to the mid-1980s. Sandstone uranium rollfront ores were processed at the mill using sulfuric acid and sodium chlorate to dissolve and oxidize uranium. Spent acids and tailings were piped in a slurry to unlined tailings ponds (Figure 6.1). The tailings fluid has a *p*H between 1.5 and 3.5, and a total dissolved solid (TDS) concentration close to 20 000 mg L^{-1}. A number of toxic metals and radionuclides are present in the tailings fluid at hazardous concentrations: arsenic (As), beryllium (Be), cadmium (Cd), chromium (Cr), lead (Pb), molybdenum (Mo), nickel (Ni), selenium (Se), radium (^{226}Ra, ^{228}Ra), thorium (^{230}Th), and uranium (^{238}U, ^{234}U). Seepage from the disposal ponds into the underlying shallow sandstone and alluvium aquifer has formed an acid plume in groundwater.

A seepage control system was installed which consisted of pumping water from wells into the tailings basin to control the further migration of the groundwater plume. The planned reclamation is to add a low-permeability cover on the tailings ponds to control

https://doi.org/10.1017/CBO9780511606274.007 Published online by Cambridge University Press

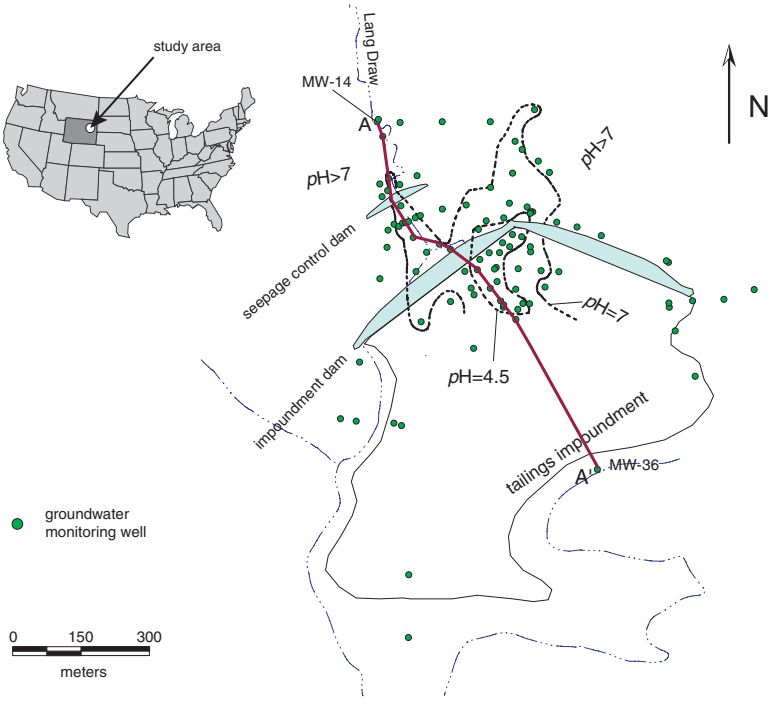

Figure 6.2. Plan view of the Bear Creek mine site and tailings impoundment.

recharge and retard further seepage into the aquifer. Hydrological modeling shows that it will take five years for the tailings fluid to drain after the low-permeability cover is installed. The aquifer contains calcite. The success of the reclamation plan depends on whether the aquifer can neutralize the acid contained in the low *p*H groundwater plume and attenuate the migration of the hazardous constituents. In other words, success depends on whether "natural attenuation" will sufficiently contain the contamination at the site once the source is terminated (see the Box on p. 110).

Figure 6.2 is a plan view of the site, showing the extent of the tailings pond, the locations of the tailings dam and seepage control dam, the size of the low *p*H groundwater plume, and the location of monitoring wells from which samples are available. Figure 6.3 is a cross-section along the line A–A′ in Figure 6.2, which is along a flow path toward the northwest. The two flow directions at the site are controlled by the site geology and delineated by the low *p*H groundwater.

6.2.2 The Purpose of Geochemical Modeling

The ultimate question for the parties and regulators responsible for the site (and the question that geochemists and hydrogeologists are hired to answer) is *what will be the concentrations of the regulated constituents at the point of compliance (POC) over the compliance period of 200 years?*

https://doi.org/10.1017/CBO9780511606274.007 Published online by Cambridge University Press

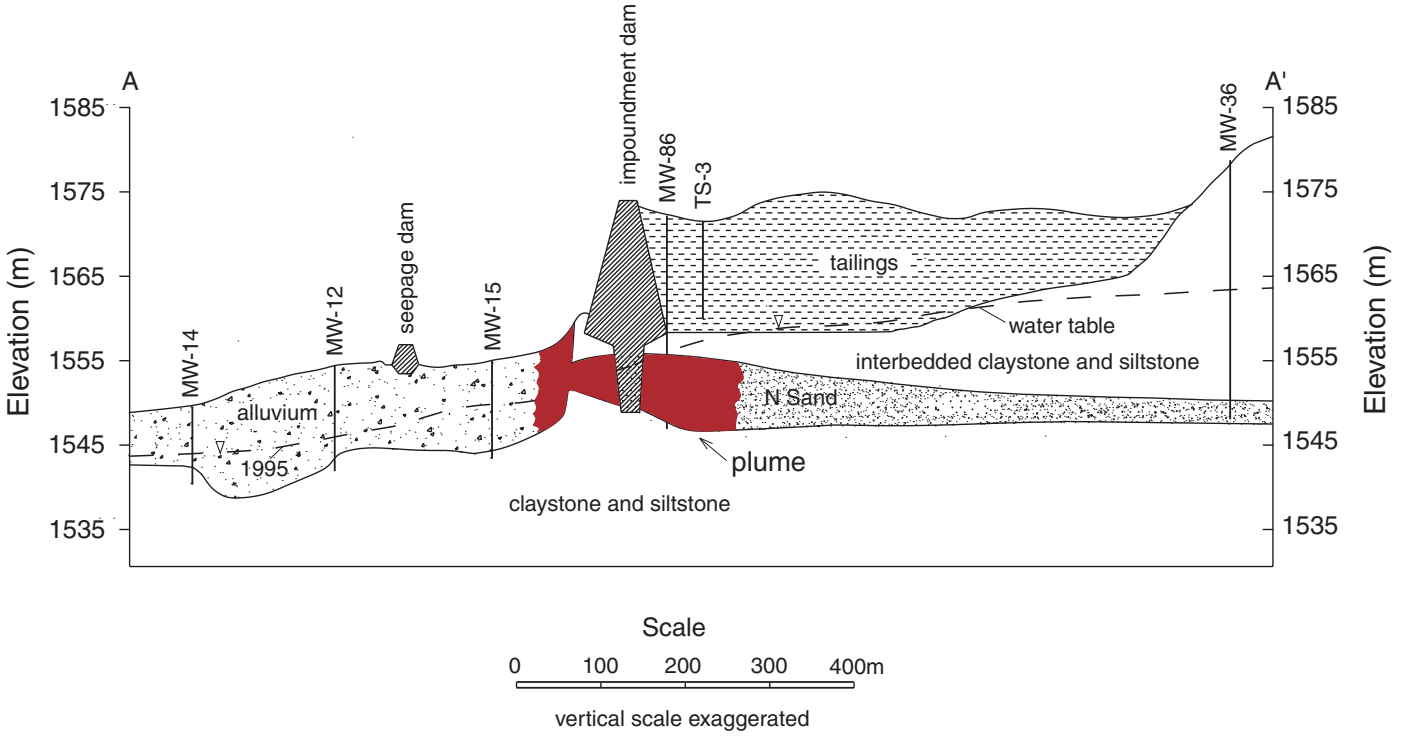

Figure 6.3. Cross-section A–A′ from Figure 6.2. Water level was recorded on January 5, 1995.

Uranium Mill Tailings

Uranium ore was mined in the USA in significant quantities by private companies to produce nuclear weaponry. After the 1950s, uranium was also needed as fuel for nuclear power plants to produce electricity. Ores are first crushed into centimeter to millimeter size. The ground ore is then disposed to the leach tanks to be dissolved and oxidized, respectively, by sulfuric acid (H_2SO_4) and sodium chlorate ($NaClO_4$). The dissolved uranium is extracted from the solutions.

The barren sand and slimes left after the leaching processes are called tailings. They contain about 85% of the radioactivity present in the unprocessed uranium ore. The tailings, spent acid, and process water are often pumped to a tailings impoundment. The tailings fluids or leachate from the tailings piles contain concentrations of radioactive and toxic materials that might pose a public health hazard.

The US Environmental Protection Agency (US EPA) developed standards to protect the public and the environment from potential radioactive and non-radioactive hazards at abandoned uranium ore processing sites (40 CFR 192). It is estimated that there are about 160 million cubic meters of mill tailings stored in temporary repositories in the USA (Miller *et al.*, 1988), and the cost for reclamation and remediation is estimated to be billions of dollars. In Canada, where a large percentage of the world's uranium was produced, it will cost about $3 billion to remediate groundwater contamination (Feasby *et al.*, 1991). Argentina, Australia, Germany, the Republic of South Africa, and Russia also have serious uranium mill tailings problems.

A number of regulations govern the concentrations that are allowed to be discharged outside of the property. These include the Nuclear Regulatory Commission's and US EPA's standards (Federal Registry 40 CFR 192), and State of Wyoming regulations for livestock and ecosystems. Recognizing the technical impracticality of controlling radionuclides at the regulated low concentrations and the fact that many uranium mill tailings impoundments are located in remote areas far from residential populations, the Nuclear Regulatory Commission allows responsible parties to petition for an Alternative Concentration Limit (ACL).

The concentrations of the hazardous constituents at the POC in the next 200 years will be the result of physical transport by the groundwater flow and chemical reactions between groundwater and the aquifer matrix. Geochemical reactions in the aquifer will obviously greatly influence the migration of the acid plume and the fate and transport of the hazardous constituents. To predict the contaminant transport accurately, these geochemical reactions should be incorporated into the transport model. The purpose of geochemical modeling, then, is to learn what geochemical reactions are possibly

Natural Attenuation

The reclamation and remediation of many contaminated sites, and uranium mill tailings sites in particular, have relied on "natural attenuation" processes. A number of physical, chemical, and biological processes can reduce the concentrations of contaminants.

- *Physical.* Dispersion, diffusion, and mixing with another water body will dilute the contaminant concentrations.
- *Chemical.* Precipitation, co-precipitation, ion-exchange, and surface adsorption can transfer contaminants from groundwater to the immobile solid phases and reduce the contaminant concentrations.
- *Biological.* Microbial mediated processes can transform organic contaminants into benign compounds or oxidize or reduce the toxic metals into a less toxic and mobile form.

A number of uranium mill tailings sites rely on "natural flushing", allowing natural groundwater movement and geochemical process to decrease contaminant concentrations. This was relied on at many of the US Department of Energy's UMTRA sites (http://www.doegjpo.com/gwwp/, October 25, 2000). This is also the strategy used at the Bear Creek site.

A scientific basis must be provided before natural attenuation can be accepted as an effective remediation alternative, because the public and communities often suspect this to be just a "do nothing" or "walk away" strategy by the polluters (National Research Council, 2000). The specific natural attenuation processes must be identified and quantified, and their long term sustainability must be evaluated (National Research Council, 2000). The geochemical modeling work, described in this section, provides the conceptual framework, which can help document and interpret the "footprints" (National Research Council, 2000) of the natural attenuation processes that are actually occurring in the aquifer.

occurring at the site, to evaluate the effects of geochemical reactions on contaminant transport, and ultimately to incorporate the results into the transport model that predicts the concentrations at the POC over the next 200 years.

6.2.3 Site Geology and Data

Numerous site monitoring data have been used to delineate four *p*H zones in the contaminated groundwater (Figure 6.2). The four zones have *p*H values of approximately 3.5, 4.5, 6.5–7.4, and $\geq$7.4, respectively (see discussion below). In designing the ground-

https://doi.org/10.1017/CBO9780511606274.007 Published online by Cambridge University Press

Analyte	Wells					
(mg L^{-1})	MW-14	MW-12	MW-15	MW-86	TS–3	MW-36
Al	< 0.5	1.15	1.33	230	1020	0.01
Ca	440	550	650	420	310	158
Fe	0.02	0.69	2.18	926	1950	0.01
Mg	59	150	250	700	1000	21
Mn	0.49	0.07	0.35	35.9	66.3	0.11
K	2	14	18	42	60	17
SiO_2	9.7	8.4	9.7	10	40.5	5.6
Na	34	265	212	278	89	61
Alkalinity as calcite	331	878	1450	<5	<5	153
SO_4^{2-}	1053	1500	1650	8100	16500	425
Cl	90	275	375	400	550	25
F	0.3	0.3	0.3	<0.1	<0.1	0.2
PO_4^{3-}	< 0.01	0.01	<0.01	0.01	0.01	<0.01
Temp. (°C)	13	12	13	12	16	15
*p*H	7.7	6.7	6.5	4.5	3.8	7.4

Table 6.1. Chemical analyses of samples from monitoring wells. The analytical data show a large excess of anions in the charge balance.

water sampling, we chose samples from locations upgradient of the acid plume, from the tailings pond, each of the *p*H zones, and a downgradient well near the property boundary. The samples are aligned along a geologic cross-section, which is depicted in Figure 6.3. The flow path is apparent not only from the *p*H contours, but also from hydrogeological data. The field parameters and major concentrations are listed in Table 6.1.

6.2.4 Selection of Modeling Code and Model Input

MINTEQA2, a geochemical modeling code published by US EPA (Allison *et al.*, 1991) was chosen for conducting speciation and solubility calculations. Program PRODEFA2, an interactive preprocessor for MINTEQA2, was used to prepare the input files, as described in §4.5.1. Special attention should be paid to the input of alkalinity data, which is discussed in Chapter 3, as well as in the MINTEQA2 manual on p. 20.

MINTEQA2 uses H_4SiO_4 as the silica component (basis species), whereas laboratories commonly report silica as SiO_2. If the units of concentration are moles per liter or moles per kilogram, no conversion factor is needed, but if units are in milliequivalents per liter, as they usually are, a concentration conversion factor of 1.6 is needed.[1]

[1] Calculated as follows:

$$\begin{aligned}\text{conc. of } H_4SiO_4 \text{ (mg L}^{-1}) &= \text{conc. of } SiO_2 \text{ (mg L}^{-1}) \times \frac{\text{mol. wt } H_4SiO_4}{\text{mol. wt } SiO_2} \\ &= \text{conc. of } SiO_2 \text{ (mg L}^{-1}) \times \frac{96.116}{60.085} \\ &= \text{conc. of } SiO_2 \text{ (mg L}^{-1}) \times 1.60\end{aligned}$$

https://doi.org/10.1017/CBO9780511606274.007 Published online by Cambridge University Press

```
12.00 MG/L   0.000  0.00000E-01
1 0 1 0 3 0 0 0 1 1 0 0 0
0   0   0
    330  0.000E-01   -7.40 y                    /H+1
     30  2.300E+02   -7.00 y                    /Al+3
    150  4.200E+02   -2.40 y                    /Ca+2
    281  9.260E+02    0.00 y                    /Fe+3
    500  2.780E+02   -2.64 y                    /Na+1
    732  8.100E+03   -2.35 y                    /SO4-2
    410  4.200E+01   -3.36 y                    /K+1
    460  7.000E+02   -3.06                      /Mg+2
    180  4.000E+02   -3.15 y                    /Cl-1
    770  1.600E+01   -4.23 y                    /H4SiO4
    270  1.000E-01   -4.98 y                    /F-1
    580  1.000E-02   -6.98 y                    /PO4-3
    140  2.458E+00  -12.07 y                    /Total CO3-2 alkali
    470  3.590E+01   -2.90                      /Mn+2

  3   1
    330     4.5000     0.0000                   /H+1
```

Table 6.2. MINTEQA2 input data for sample MW-86, produced by PRODEFA2.

For low *p*H water samples from the plume, concentrations of carbonate species were not measured, but they should be low. In modeling, we assumed that TS-3 and MW-86 have a small amount of dissolved carbonate. As an example of the MINTEQA2 input files, Table 6.2 shows the input file for sample MW-86, prepared by using PRODEFA2.

6.2.5 Geochemical Modeling

The overall aim is to use chemical analyses of the groundwater to determine what chemical reactions between the water and the host aquifers are probably occurring as the water moves along the aquifer. If the factors controlling the acidity and metal content are understood, predictions concerning them are easier to make. To do this we will:

- calculate the activities of all dissolved species in each sample;
- calculate the Saturation Indices (SI) of important minerals, and plot them on the cross-section along the flow path toward the northwest;
- observe a stepwise change in *p*H of the solutions, and test a buffering hypothesis with a titration model;
- plot the samples on activity–activity diagrams for additional insight.

https://doi.org/10.1017/CBO9780511606274.007 Published online by Cambridge University Press

6.2.6 Modeling Results

The calculated concentrations for selected species are shown in Table 6.3, and the Saturation Indices are listed in Table 6.4. These results on aqueous speciation are plotted in Figure 6.4, and show the aqueous speciation or species distribution along the cross-section A–A′.

The distribution of species varies along the flow path because the water chemistry changes drastically. The upgradient and hence background, uncontaminated water (MW-36) is a Ca^{2+}–HCO_3^- type water with a *p*H slightly higher than neutral, while the tailings fluid (TS-3) is predominantly SO_4^{2-}-rich, with high concentrations of dissolved metals Al, Fe, Mg, and Na. Contaminated water downgradient from the tailings pond has elevated SO_4^{2-}, but the metal concentrations have dropped significantly. The aqueous speciation is thus controlled by both solution *p*H and major ion concentrations.

Comments on Results for Specific Components

The following are a few of the more important speciation modeling results.

Al^{3+} The dominant species are Al^{3+}–SO_4^{2-} complexes in low *p*H, high SO_4^{2-} water (TS-3, MW-86) and $Al(OH)_3^\circ$ in low SO_4^{2-} and near neutral waters (MW-36, MW-15, MW-12, MW-14). It is wise to bear in mind that accurate analyses for dissolved Al are very difficult to perform. Because of its very low dissolved concentrations, particulate and colloidal particles containing Al can dominate an analysis, unless great care is taken. Driscoll and Postek (1996) note that " . . . because particulate minerals exhibit a continuous size distribution, no absolute distinction between dissolved and particulate forms can be made, and results show a strong dependence on filter pore size". In the absence of other errors, analyses for Al should be regarded as maximum possible values, from the point of view of geochemical modeling. It should also be noted that if an Al content is not reported (commonly the case), no conclusions at all can be reached about the saturation state of any aluminosilicate mineral.

Fe^{3+} Modeling results indicate the dominance of the polynuclear hydroxy-complexes $Fe_3(OH)_4^{5+}$ in low *p*H, high Fe^{3+} solutions (about $\geq 10^{-2}$ molal). See Stumm and Morgan (1996) for a discussion of these polynuclear complexes. Notably, the trimer is dominant over Fe^{3+}– SO_4^{2-} complexes. In near neutral solutions, the species $Fe(OH)_2^+$ is dominant.

6.2.7 Analysis of Mineral Saturation Indices

Figures 6.5–6.9 show the calculated Saturation Indices (SI) for carbonate, sulfate, iron, aluminum, and manganese minerals at Bear Creek. The calculation results show that a number of minerals are supersaturated in our samples. However, not all minerals that are indicated to be supersaturated are actually present at the site. Our discussion here is thus focused on how to interpret the calculated SI values, or to identify the mineral phases that are most likely relevant to the system.

https://doi.org/10.1017/CBO9780511606274.007 Published online by Cambridge University Press

Component	Species	MW-36	TS-3	MW-86	MW-15	MW-12	MW-14
Mn+2	Mn+2	82.1	52.7	58.6	71.3	72.8	75.7
	MnSO4 AQ	16.1	46.4	40.6	18.8	20.6	21.2
	MnHCO3 +	1.7	0	0	8.7	5.7	2.6
Al+3	Al+3	0	20	26.6	0	0	0
	Al(OH)2 +	2.9	0	0	22.8	15.9	1.5
	Al(OH)4 -	17.4	0	0	1.3	1.7	20.8
	Al(OH)3 AQ	79.7	0	0	70.4	79	77.7
	AlSO4 +	0	28.8	32.4	0	0	0
	Al(SO4)2 -	0	51.1	40.1	0	0	0
	AlF +2	0	0	0	3.1	1.6	0
Ca+2	Ca+2	80.6	49.4	55	72.8	72.8	74
	CaSO4 AQ	18.4	50.6	45	22.6	24.3	24.4
	CaHCO3 +	0	0	0	4.5	2.9	1.3
Fe+3	FeOH2 +	75.1	5.4	34.8	97	95.2	56.1
	FeOH3 AQ	19.3	0	0	2.8	4.4	27.3
	FeOH4 -	5.6	0	0	0	0	16.6
	FeSO4 +	0	10.1	1.7	0	0	0
	Fe(SO4)2 -	0	7.1	0	0	0	0
	Fe2(OH)2+4	0	7.4	2.7	0	0	0
	Fe3(OH)4+5	0	64.7	56	0	0	0
	FeOH +2	0	4.2	3.8	0	0	0
Na+1	Na+1	99	90.1	0	0	97.6	98.1
	NaSO4 -	0	9.9	0	0	2	1.7
SO4-2	SO4-2	79.6	51.1	66.6	65.7	68.6	70.5
	MgSO4 AQ	3.2	11.3	14.3	11.9	8.5	4.9
	CaSO4 AQ	16.4	2.3	5.6	21.3	21.3	24.4
	AlSO4 +	0	6.3	3.3	0	0	0
	Al(SO4)2 -	0	22.5	8.1	0	0	0
	FeSO4 +	0	2.1	0	0	0	0
	Fe(SO4)2 -	0	2.9	0	0	0	0
	NaSO4 -	0		1	0	1.5	0
K+1	K+1	98.8	87.8	0	0	97.6	97.9
	KSO4 -	1.2	12.2	0	0	2.4	2.1
Mg+2	Mg+2	82.2	52.7	0	0	73.8	75.8
	MgHCO3 +	1.2	0	0	0	4.6	2
	MgSO4 AQ	16.5	47.3	0	0	21.6	21.9
Cl-1	Cl-1	100	99.9	100	100	100	100
H4SiO4	H4SiO4	99.8	100			100	99.6
F-1	F-1	96.7	0	0	0	77.5	93.6
	MgF +	2	0	0	0	6.8	4
	CaF +	1.3	0	0	0	2.1	2.5
	AlF +2	0	99.4	0	0	4.2	0
	AlF2 +	0	0	0	0	5	0
	AlF3 AQ	0	0	0	0	4.2	0
PO4-3	H2PO4 -	21.1	9.3	0	0	42.5	8.3
	MgHPO4 AQ	7	1.5	0	0	10.7	10.5
	CaHPO4 AQ	23	0	0	0	17.2	33.9
	CaH2PO4 +	0	0	0	0	3.5	0
	CaPO4 -	1.3	0	0	0	0	3.8
	HPO4 -2	46.1	0	0	0	23.6	41.4
	FeH2PO4 +2	0	88.9	0	0	0	0
	MgH2PO4 +	0	0	0	0	2	0
	MgPO4 -	0	0	0	0	0	1.2
Ba+2	Ba+2	100	100	100	100	100	100
CO3-2	CaHCO3 +	1.3	0	0	2.1	2.1	2.6
	HCO3 -	91.4	0	2.3	64.3	73.4	92.4
	H2CO3 AQ	6.5	99.5	97.6	31.3	22.7	3
	MgHCO3 +	0	0	0	2.1	1.5	0

Table 6.3. Species distributions (%) in monitoring wells.

https://doi.org/10.1017/CBO9780511606274.007 Published online by Cambridge University Press

NAME	MW-36	TS-3	MW-86	MW-15	MW-12	MW-14
CA-NONTRONIT	24.75	26.057	26.94	27.875	27.09	28
MG-NONTRONIT	24.341	25.882	26.718	27.543	26.733	27.592
K-NONTRONITE	18.735	20.224	21.028	21.787	20.976	21.617
NA-NONTRONIT	17.949	19.527	20.332	21.172	20.429	21.054
MUSCOVITE	5.195	0.98	4.081	11.548	11.249	10.633
KAOLINITE	3.856	3.154	4.888	8.729	8.476	7.939
PYROPHYLLITE	3.611	5.055	5.896	9.576	9.288	8.772
DIASPORE	1.973	0.524	1.949	3.921	3.84	3.533
HALLOYSITE	0.474	-0.215	1.471	5.324	5.059	4.535
BOEHMITE	0.179	-1.261	0.127	2.108	2.018	1.721
GIBBSITE (C)	0.123	-1.334	0.112	2.079	2.004	1.692
LOW ALBITE	-1.499	-2.529	-2.352	1.434	1.484	1.456
ANALCIME	-1.531	-3.668	-2.914	0.92	1.02	0.949
ALOH3(A)	-1.595	-3.041	-1.64	0.339	0.252	-0.048
LAUMONTITE	-1.657	-7.56	-5.627	2.63	2.563	4.157
ANALBITE	-2.479	-3.503	-3.353	0.44	0.483	0.462
Al2O3	-4.034	-7.06	-3.689	0.122	0.093	-0.653
KALSILITE	-4.358	-7.862	-6.544	-2.905	-2.964	-3.03
ANORTHITE	-4.675	-12.751	-9.771	-1.397	-1.39	0.143
NEPHELINE	-5.061	-8.286	-7.01	-3.116	-2.979	-3.08
WAIRAKITE	-6.39	-12.255	-10.459	-2.169	-2.271	-0.643
SPINEL	-8.231	-17.091	-13.33	-5.501	-5.559	-4.395
CRYOLITE	-19.168	-34.164	-32.062	-14.299	-12.872	-18.311
GEHLENITE	-20.916	-37.464	-32.709	-19.742	-19.436	-15.863
JAROSITE K	4.443	16.237	16.952	9.123	7.446	4.293
JAROSITE NA	1.504	13.579	14.246	6.673	5.19	2.004
BARITE	0.787	1.466	1.428	0.967	1.018	0.989
GYPSUM	-0.553	0.217	0.296	0.164	0.127	0.024
ANHYDRITE	-0.867	-0.081	-0.047	-0.169	-0.218	-0.31
ALUNITE	-1.123	7.633	10.206	8.46	7.736	2.625
AL4(OH)10SO4	-2.291	-0.105	5.093	8.147	7.694	4.126
EPSOMITE	-3.848	-1.691	-1.869	-2.664	-2.84	-3.251
ALOHSO4	-4.779	1.956	2.092	-0.574	-0.983	-3.433
MIRABILITE	-6.361	-4.021	-4.207	-4.957	-4.691	-6.564
THENARDITE	-7.792	-5.378	-5.783	-6.488	-6.274	-8.098
MNSO4	-11.757	-8.647	-8.922	-11.25	-11.948	-11.056
ALUM K	-16.162	-4.41	-5.163	-10.722	-11.407	-15.779
FE2(SO4)3	-43.244	-19.405	-22.302	-36.166	-38.108	-43.686
HEMATITE	17.507	16.527	18.581	18.356	17.672	18.251
MAGHEMITE	7.898	6.836	9.217	8.91	8.308	8.805
MAG-FERRITE	7.246	0.292	3.3	6.951	6.381	8.727
FEOH)2.7CL.3	6.999	7.924	8.867	8.114	7.715	7.523
GOETHITE	6.273	5.78	6.817	6.703	6.363	6.65
LEPIDOCROCIT	5.771	5.239	6.43	6.277	5.976	6.224
JAROSITE K	4.443	16.237	16.952	9.123	7.446	4.293
FERRIHYDRITE	2.251	1.716	2.909	2.756	2.455	2.704
JAROSITE H	-2.841	12.198	12.09	2.637	0.798	-2.463
CALCITE	-0.026	-7.644	-6.04	0.374	0.309	0.889
ARAGONITE	-0.2	-7.813	-6.226	0.193	0.123	0.708
DOLOMITE	-0.761	-14.578	-11.719	0.466	0.176	1.048
MAGNESITE	-1.228	-7.429	-6.166	-0.398	-0.621	-0.332
RHODOCHROSIT	-1.379	-6.702	-5.289	-1.11	-1.794	-0.26
NESQUEHONITE	-3.627	-9.836	-8.565	-2.796	-3.018	-2.729
WITHERITE	-3.796	-11.499	-10.055	-3.956	-3.944	-3.279
HUNTITE	-6.438	-32.643	-27.312	-3.577	-4.328	-2.864
ARTINITE	-8.009	-20.228	-17.866	-8.255	-8.328	-6.306
NATRON	-9.288	-15.338	-14.013	-8.211	-7.975	-9.161
THERMONATR	-11.195	-17.174	-16.057	-10.212	-10.027	-11.165
HYDRMAGNESIT	-17.542	-48.352	-42.253	-15.323	-16.079	-13.175

Table 6.4. Calculated Saturation Indices for selected minerals.

https://doi.org/10.1017/CBO9780511606274.007 Published online by Cambridge University Press

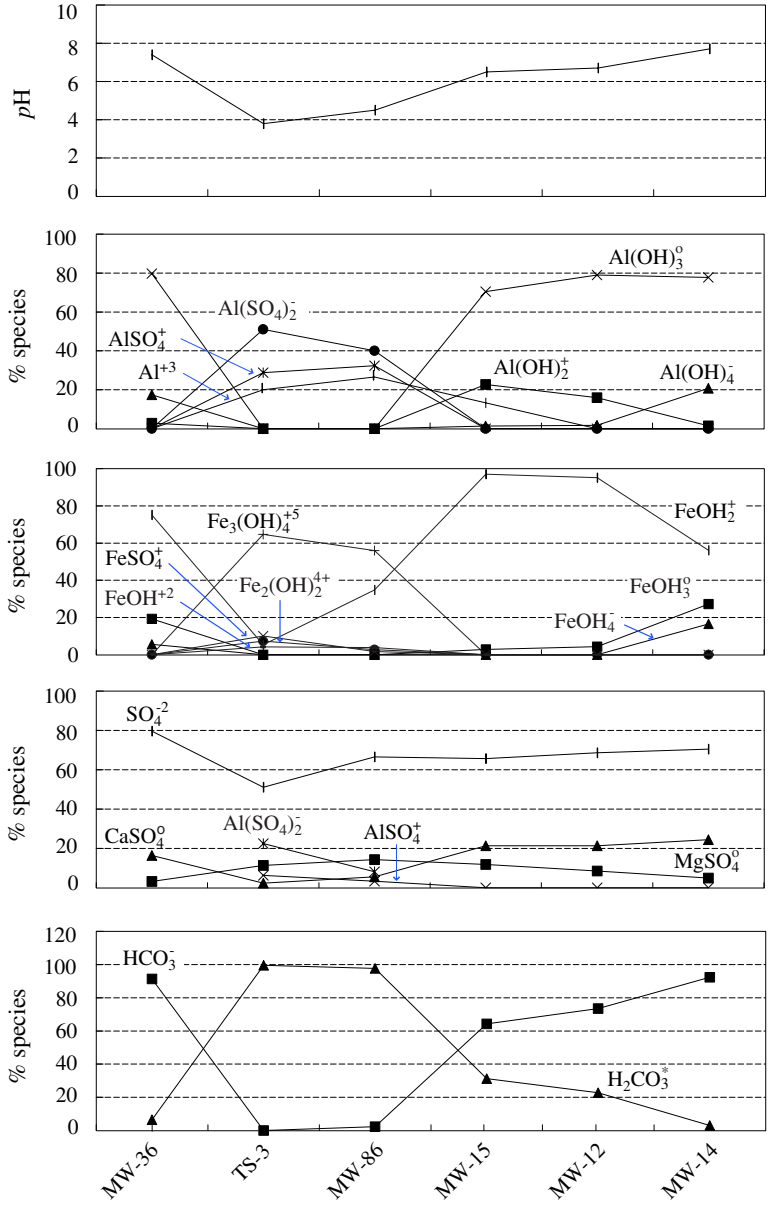

Figure 6.4. Changes of species distribution in groundwater samples from cross-section A–A′ from Figure 6.3.

https://doi.org/10.1017/CBO9780511606274.007 Published online by Cambridge University Press

The decision as to which mineral phases are significant in a system based on modeling results is a common problem for geochemists. Speciation–solubility modeling only can point out the possibilities of solubility control. Positive identification of the solubility limiting phases can only be accomplished by microscopic or X-ray analysis of soils and aquifer matrix. As we pointed out earlier, mineralogical work is often not a part of groundwater studies. One reason for this is that it is difficult work, given the often extremely fine-grained or amorphous phases and solid solution effects (Jambor and Blowes, 1994). In these cases, the modeler's geological knowledge becomes significant. Modelers can also refer to mineralogical studies with similar geological and environmental conditions.

Given accurate analyses and thermodynamic data, Saturation Indices can only show which minerals could conceivably precipitate from the solution ($SI>0$) (and could therefore be present in the system), and which minerals absolutely could not ($SI<0$). There are several reasons why many of the minerals which are calculated to be supersaturated may not actually be present in the system.

- Minerals which are indicated to either dissolve or precipitate may actually not do so because of kinetic constraints. This applies especially to precipitation of complex structures which may form quite easily at higher temperatures. Quartz is almost universally supersaturated in surface waters, and if SiO_2 does precipitate, it will be in some other form, such as amorphous silica.

- Calculated SI are for pure "end-member" minerals, but the actual minerals in environmental settings can be solid solutions with complicated compositions. Alpers *et al.* (1989) found that, for jarosite, errors of more than one order of magnitude can be introduced by ignoring solid solutions.

- The magnitude of the SI is often of little importance. Bethke (1996) and Wolery (1992) point out that the SI value depends not only on the concentrations involved, but on the formula of the mineral. For example, if we were to write the formula of quartz as Si_2O_4 instead of SiO_2, its Saturation Index would be doubled. The choice of large formula units for clays and zeolites explains why these minerals often occur at the top of the supersaturation list (Bethke, 1996, p. 91).

- Errors in analyses may be significant. We have already mentioned the problem with particulate and colloidal aluminum, and the same point could be made about silica and many other elements present in small amounts.

- The reliability of much of the thermodynamic data is always questionable. The data are obtained in a number of different ways, some more reliable than others. For solid phases, the nature of the solid phases involved in the determination of the data may be different from those in the system from the point of view of grain size, crystallinity, defect structure, and composition.

- Of course, even if the calculated SI is accurate, e.g., a given mineral is in fact present and is dissolving ($SI < 0$), or is in fact precipitating ($SI > 0$), the SI tells us nothing at all about the rate at which this is happening, nor about the quantities of minerals involved.

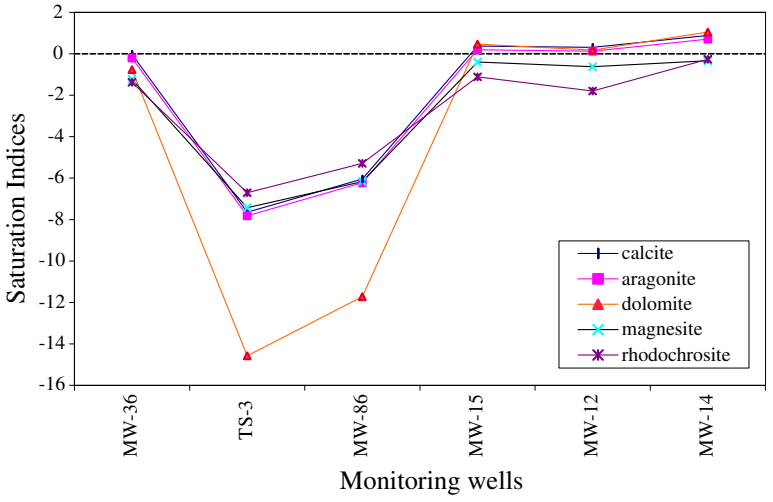

Figure 6.5. Saturation Indices for carbonate minerals from MINTEQA2.

On the other hand, many investigations have shown that Saturation Indices are a reasonably good guide to certain phases, such as some carbonate and sulfate minerals. Saturation Indices are also quite useful in reaction path modeling (Chapter 8) and inverse mass balance modeling (Chapter 9) in the sense that they indicate (within the accuracy of the data) which processes are possible (e.g., precipitation of a phase having an SI > 0), and which are impossible (e.g., dissolution of a phase having an SI > 0).

Carbonate Minerals (Figure 6.5) SI values of calcite for the upgradient well MW-36, and wells downgradient from the plume MW-15 and MW-12 water are within 0 ± 0.5, a range well within the uncertainties propagated from errors associated with sampling, laboratory analyses, and thermodynamic properties. MW-14 shows an SI of 0.9. Equilibrium with calcite at the site is easy to be inferred because we know that the N sand and alluvium contain about 2% calcite. Calculated SI values for aragonite are within 0 ± 0.2, but its presence is unlikely. Modeling results also show supersaturation or equilibrium with dolomite in waters downgradient from the plume, but dolomite is undersaturated in the upgradient water (MW-36). Whether or not dolomite is present in the sandstone is not independently confirmed, but precipitation of ordered dolomite would be rather unusual under surface conditions. In all water samples, magnesite ($MgCO_3$) is undersaturated.

Sulfate Minerals (Figure 6.6) Fifteen sulfate minerals are present in the thermodynamic database. The calculations show that many are supersaturated in our water samples. Several members of the alunite–jarosite group are grossly supersaturated, but alunite and jarosite are known to be supersaturated without precipitating in some acidic surface waters (Alpers *et al.*, 1994). Aluminum hydroxy sulfates, $Al(OH)SO_4$ (jurbanite), and $Al_4(OH)_{10}SO_4$ (basaluminite), are also supersaturated at some points

https://doi.org/10.1017/CBO9780511606274.007 Published online by Cambridge University Press

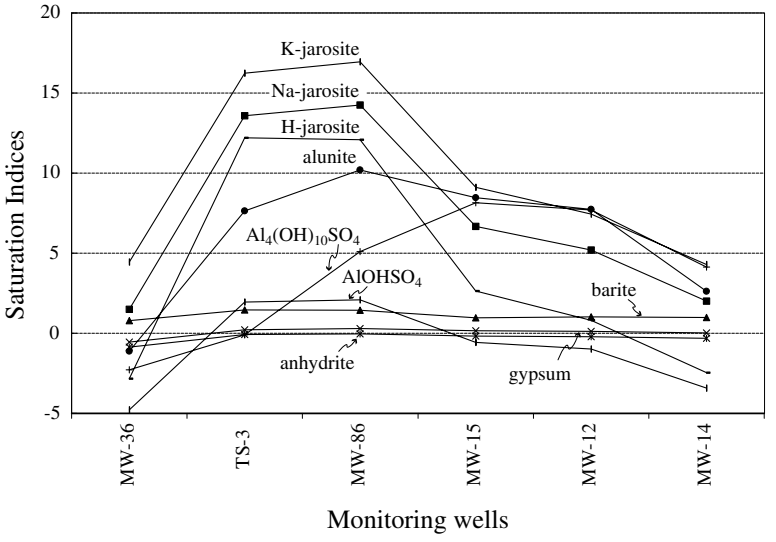

Figure 6.6. Saturation Indices for sulfate minerals from MINTEQA2.

in the cross-section. These minerals have been found in mine drainage settings (Alpers *et al.*, 1994). Stollenwerk (1991) found that using a modified jurbanite solubility product fitted well with the Al results in column experiments on Pinal Creek acid water at $p\mathrm{H} < 4.7$. On the other hand, mineralogical studies of acid mine drainage sites indicate that gypsum is the most common sulfate phase controlling sulfate concentrations in such environments (Davis *et al.*, 1991; Jambor and Blowes, 1994).

Iron Minerals (Figure 6.7) The calculations show that a number of iron minerals are supersaturated in the fluids. Besides jarosite, the water samples are also supersaturated with goethite and hematite, both of which have slow growth kinetics at surface temperatures. Jambor and Blowes (1994) argue that goethite with various crystallinities is the iron phase that commonly controls iron solubilities. Our calculations show that SI values for ferrihydrite, defined in the MINTEQA2 database as an amorphous $Fe(OH)_3$, are closer to zero than are those for well crystallized goethite. Its SI values are about two log units above zero. These SI, however, are a function of the log K values in the database. The equilibrium constants for amorphous iron hydroxide or oxide vary several orders of magnitude (Cornell and Schwertmann, 1996; Stumm and Morgan, 1981, p. 240). MINTEQA2 uses a value of K_{sp} of -4.89 from Nordstrom *et al.* (1990), but the NBS value reported by Wagman *et al.* (1982) is -5.66.

Aluminum Minerals (Figure 6.8) Similarly, a large number of aluminum minerals are supersaturated in the sampled water. The sandstone and alluvium materials contain aluminum silicate minerals and clays, but these minerals are unlikely to be at equilibrium in groundwater due to kinetic inhibitions. The calculated SI for clays are again for end-members. In our samples, gibbsite or an amorphous analog appears to be the

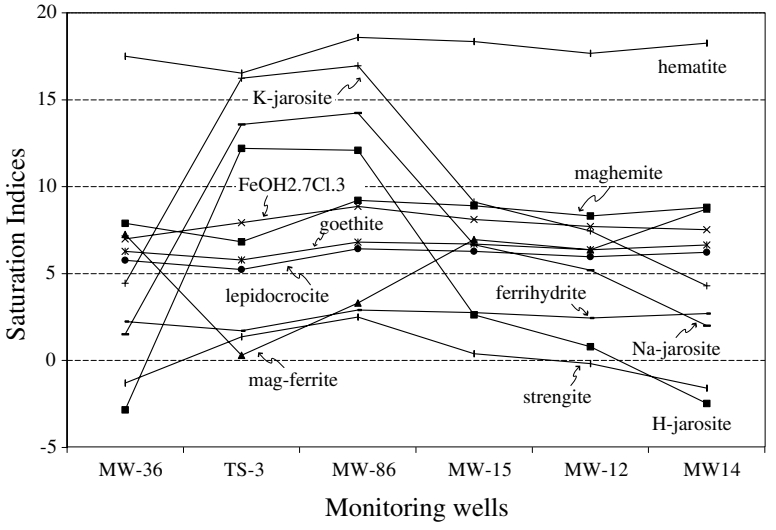

Figure 6.7. Saturation Indices for iron-bearing minerals from MINTEQA2.

closest to equilibrium. It is fairly common to find that the Al^{3+} content of soil waters is apparently controlled by the solubility of a gibbsite-like mineral, although gibbsite is rarely identified mineralogically (Hendershot *et al.*, 1996). This may be due to an amorphous gibbsite-like phase, or to surface adsorption effects. Stollenwerk (1991) found that using $Al(OH)_3(a)$ from MINTEQA2 and a modified log K for jurbanite successfully explained solubility control of his experimental data. Jurbanite controls Al solubility at $p\mathrm{H} < 4.7$ and $Al(OH)_3(a)$ controls solubility at $p\mathrm{H} > 4.7$.

Mn Minerals (Figure 6.9) All water samples are undersaturated with respect to all Mn^{2+}-containing mineral phases available in the MINTEQA2 thermodynamic database. However, along the flow path the Mn concentrations drop from highly contaminated to only slightly contaminated groundwater, so that Mn must have been precipitated in some form. The most likely precipitate in surfacial environments is MnO_2 (Hem, 1985), but the small amount of Mn involved may simply have been adsorbed on mineral surfaces.

6.2.8 Activity–Activity Diagrams

Additional insight into the reactions involved is obtained by plotting the solution compositions on appropriate activity–activity diagrams (Figure 6.10). This is most conveniently done with programs in the The Geochemist's Workbench™ group (Bethke, 1994), because they are among the few geochemical modeling programs that can produce diagrams. However, the same diagrams can be produced from the output of other programs with a little more effort.

Notice in Figure 6.10 how the upgradient background (MW-36) fluid plots higher in the diagram, and the more contaminated fluids (MW-86, TS-3) plot lower, because

https://doi.org/10.1017/CBO9780511606274.007 Published online by Cambridge University Press

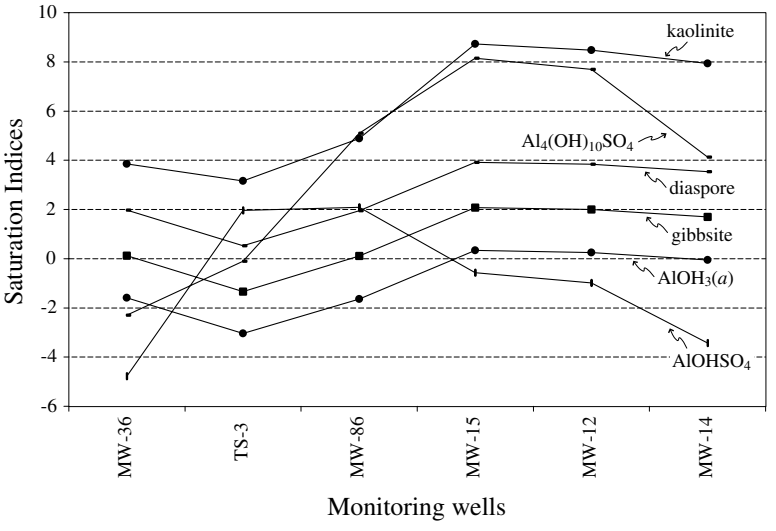

Figure 6.8. Saturation Indices for aluminum-bearing minerals from MINTEQA2.

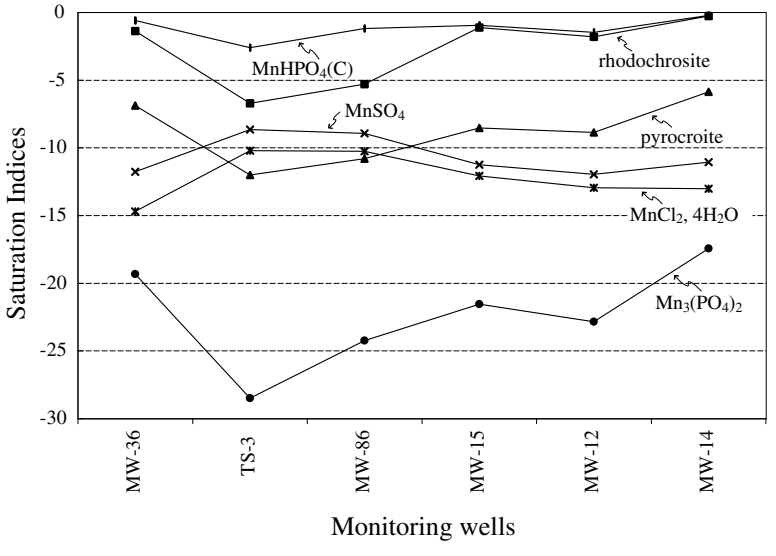

Figure 6.9. Saturation Indices for Mn-bearing minerals from MINTEQA2.

https://doi.org/10.1017/CBO9780511606274.007 Published online by Cambridge University Press

"Downstream Equilibrium Conditions"

In analysis of Saturation Indices, it is tempting to infer that minerals are present in the regions where SI ≥ 0. However, Walsh *et al.* (1984) noted that fluid in the downstream direction of a set of minerals is saturated with respect to this set of minerals even though the solids themselves are not present in the downstream region. They termed this condition the "downstream equilibrium condition". It is a result of physics and thermodynamics, under the imposed local equilibrium assumption (Lichtner, 1996; Walsh, 1983).

If we examine the SI values at the Bear Creek Uranium site, we see that the uncontaminated background groundwater is undersaturated with respect to gypsum (SI < 0, MW-36 in Figure 6.6). The acidic groundwater (MW-86) in the $Al(OH)_3(a)$ buffer zone has a SI ≈ 0, and, according to our geochemical evolution model, there should be gypsum present in the plume. The calcite dissolution–gypsum precipitation front should be located somewhere between MW-86 and MW-15, judging from the *p*H of the samples (4.5 and 6.5, respectively). However, samples downstream from the gypsum precipitation zone, MW–15, MW-12, and MW-14 all have SI ≈ 0. This distribution of SI values may indicate the "downstream equilibrium condition", rather than the presence of gypsum in these areas, which we know is not present in the alluvium. We note that gypsum precipitation is fast and that the local equilibrium assumption is probably valid.

larger values of a_{H^+} (lower *p*H) produce lower values of the ratio a_{K^+}/a_{H^+}. The more contaminated fluids also have a greater silica content and so plot more to the right.

Figure 6.10 shows solution compositions (at least the $\log a_{K^+}/a_{H^+}$ and $\log a_{SiO_2(aq)}$ aspects of the compositions) calculated by MINTEQA2 plotted on mineral boundaries calculated by The Geochemist's Workbench™. It is desirable not to mix databases in this way. To show the differences between these databases, Figure 6.11 shows the mineral boundaries calculated from both MINTEQA2 and The Geochemist's Workbench™. These differences are typical of those one can expect by changing databases.

6.2.9 Geochemical Evolution Along A Flow Path

The speciation–solubility modeling results, combined with other numerous groundwater data that are presented here, and knowledge of water–rock interactions, help to conceptualize geochemical evolution along the flow path. As discussed earlier, groundwater monitoring data and geochemical modeling have delineated four geochemically distinct zones. The existence of geochemical zones is mainly supported by the observation that the *p*H distribution is discontinuous. Distinct *p*H zones are also observed at many other acid mine drainage environments (Morin *et al.*, 1988), and is explained by

https://doi.org/10.1017/CBO9780511606274.007 Published online by Cambridge University Press

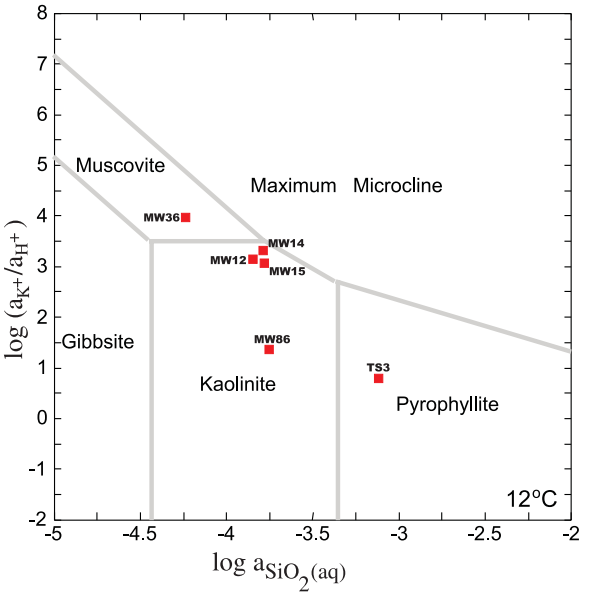

Figure 6.10. Projection of water sample compositions (calculated by MINTEQA2) onto the log a_{K^+}/a_{H^+} vs. log $a_{SiO_2(aq)}$ diagram at 12°C.

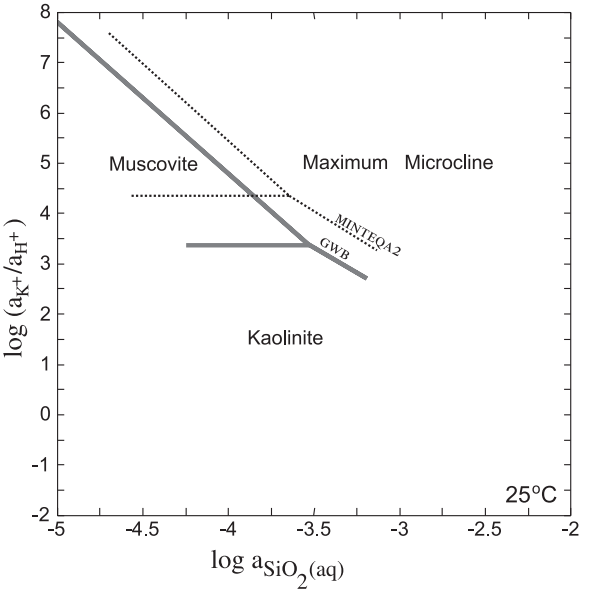

Figure 6.11. The same curves as drawn by The Geochemist's Workbench™ and from the data in MINTEQA2, at 25°C.

https://doi.org/10.1017/CBO9780511606274.007 Published online by Cambridge University Press

the successive buffering process discussed in §8.4.

Based on this conceptual model and site data, we can decipher the groundwater geochemical evolution along the flow path in cross-section A–A′ (Figure 6.3). Groundwater at MW-14 has not yet been impacted by acid as indicated by its relatively high *p*H, but higher concentrations of metals and Cl^- and SO_4^{2-} have already reached the area (see Table 6.1 and compare concentrations). Groundwater at MW-15 and MW-12 are at the first stage of sulfuric acid intrusion. Calcite in the aquifer reacts with the infiltrating low *p*H water and buffers the fluid *p*H to above 6.5:

$$CaCO_3 + H^+ = Ca^{2+} + HCO_3^-$$

As long as calcite is present, the *p*H will be maintained at about 6.5 while calcite in the aquifer matrix is being consumed. This reaction is evident from the higher Ca^{2+} and HCO_3^- concentrations compared with those in background water as represented by MW-36.

The dissolution of calcite also results in higher calcium concentration and leads to gypsum precipitation:

$$Ca^{2+} + SO_4^{2-} + 2H_2O = CaSO_4 \cdot 2H_2O$$

As a result, sulfate concentrations are reduced, compared with those in upgradient water.

Groundwater at MW-86 is at the second geochemical phase when calcite in the aquifer is depleted. The fluid *p*H of the groundwater is reduced to about 4.5 and is buffered by amorphous aluminum hydroxide or kaolinite.

$$Al^{3+} + 3H_2O = Al(OH)_3(aq) + 3H^+$$

Precipitation reduces the aluminum and iron concentrations in the fluid to a few milligrams per liter. The fact that there are few observed groundwater *p*H values between 6.5 and 4.5 supports the hypothesis that solid phases buffer fluid *p*H at the site.

The *p*H of tailings fluids (TS-3) appears to be controlled by iron hydroxide:

$$Fe^{3+} + 3H_2O = Fe(OH)_3(aq) + 3H^+$$

The fluid is undersaturated with respect to gibbsite or amorphous Al hydroxide. As more tailings fluids seep into the shallow aquifer, the reaction zones will shift downgradient.

6.2.10 Comments on the Bear Creek Site

The speciation and solubility modeling of six water analyses gives us:

- six snapshots of the speciation of cations and anions in the aqueous phase and the equilibrium state with respect to minerals in a dynamic system;
- identifcation of the major chemical reactions that control the acid plume migration;
- a conceptual model of geochemical evolution along the flow path at the site;

https://doi.org/10.1017/CBO9780511606274.007 Published online by Cambridge University Press

- identified reactions that can be significant to heavy metal and radionuclide retardation.

The modeling results show that a large amount of iron and aluminum hydroxide will be precipitated. Coprecipitation with iron and aluminum hydroxide is commonly found and is a significant natural attenuation process (Herbert, 1996; National Research Council, 2000; Zhu *et al.*, 1993).

In terms of answering the ultimate question "what concentrations will be at the point of compliance over the next 200 years?", the speciation–solubility calculations appear to provide only tentative results. The Saturation Indices only provide information about the equilibrium state, but do not consider masses or the processes that are needed for the aquifer to neutralize the acid plume. The equilibrium modeling also provides only a snapshot of the state of equilibrium in a dynamic system, in which the controlling reactions vary over time and space. Besides geochemical reactions, the potential migration of acid and metals is also influenced by factors such as advection and hydrodynamic dispersion. Does that mean that geochemical modeling is not useful? Not at all. A good analog of our speciation–solubility results is the equal-potentiometric surfaces prepared for a groundwater flow model. The potentiometric surfaces themselves do not provide answers to all practical questions regarding groundwater flow, but they do provide a basis for constructing a conceptual flow model. While the potentiometric surfaces indicate the possible directions of the groundwater flow, Saturation Indices point out the possible directions of chemical reactions. Similarly, the equilibrium reactions between aquifer matrix and groundwater characterized from speciation–solubility modeling at a site provide a geochemical basis for any meaningful contaminant transport models.

6.3 Applications to Bioavailability and Risk Assessment Studies

Davis *et al.* (1992, 1993, 1996) and Hemphill *et al.* (1991) contend that geochemical factors control the bioavailability of lead (Pb) and arsenic (As) and that human risk assessments based on the assumption that soil Pb and As are equally bioavailable as soluble salts are flawed. When soluble salts, for example $Pb(OAc)_2$, are used in toxicological studies, the amount of Pb in body fluids is controlled by supplied salt mass. For mine-waste impacted soils, not all Pb and As are soluble. In fact, the solubility may be much less and is controlled by geochemical factors that include the dominant metal-bearing phases, encapsulation, and rinding by less soluble phases, and particle sizes. They reasoned that soil Pb and As should be less bioavailable than soluble salts because Pb and As in the mining wastes are less soluble. Bioavailability is expressed as the percentage of ingested materials absorbed through the intestinal wall into the systemic blood system. The mineralogical controls can help to explain the variable blood Pb levels in different settings (urban, smelter, and mining waste) with similar soil Pb levels.

Davis *et al.* (1992, 1993) first studied the mineralogy of the mining waste impacted soil in the Butte, Montana, mining district, and then performed speciation–solubility calculations. They reasoned that dissolution of As and Pb under the acidic stomach

Solid phase	Solubility	Distribution %
Galena (PbS)	69 mg/L	72 Pb^{2+}
		28 $PbCl^{+}$
Anglesite ($PbSO_4$)	69 mg L^{-1}	66 Pb^{2+}
		26 $PbCl^{+}$
		4 $PbCl_2^{\circ}$

Table 6.5. Solubility control of lead concentrations in stomach fluids (*p*H 2.0, 0.01 M HCl, and *Eh* +200 mV. Calculated using MINTEQA2 (Davis *et al.*, 1992).

.

conditions is the necessary precursor for absorption of these metals by the small intestine. Therefore, solubility of Pb and As from equilibrium modeling is intended to provide an upper bound of bioavailable Pb and As in the gastrointestinal (GI) tract.

Davis *et al.* (1992, 1993) used MINTEQA2 for their solubility calculations. The stomach fluid is simulated by using a 0.01 M HCl solution at a *p*H of 2.0 under an oxidizing condition of *Eh* of 200 mV, and the small intestinal fluid by a *p*H of 7.0 and Cl^- of 10^{-7} M. The minerals anglesite ($PbSO_4$) and enargite (Cu_3AsS_4) are believed to be the most likely phases controlling Pb and As solubility. The calculated solubility of anglesite is 69 mg L^{-1} in stomach fluid and 37 mg L^{-1} in the small intestine. Addition of 10^{-4} M each of acetate and citrate acids increase the solubility of Pb to 61 mg L^{-1} in the small intestine because of the formation of organic acid–Pb complexation. Addition of phosphate and calcium caused the precipitation of lead phosphate phases and a lower solubility control. Table 6.5 lists the calculated solubility and aqueous species distribution.

For As solubility calculations, the modeling generated less useful information. Enargite is found to be quite soluble in stomach fluids. Davis *et al.* (1992) believe that dissolution kinetics or inhibition from reaction with GI fluids by encapsulation with less soluble phases (e.g. jarosite) cause the observed discrepancy between equilibrium calculations and experiments.

Comparing the modeling results with *in vivo* experiments using female New Zealand white rabbits shows that the *in vivo* Pb concentration is lower than the up-bound of soluble Pb calculated from anglesite solubility in stomach fluid. The calculated Pb solubility is 69 mg L^{-1}, whereas the *in vivo* Pb concentration in the rabbit stomach fluid is 8.5 mg L^{-1}. Ruby *et al.* (1992) attributed the lower experimental Pb concentration to dissolution kinetics of anglesite and a short transit time in the GI tract (6 hours).

While Davis and his colleagues illustrated the significance of soil metal speciation in risk assessment, Morrison *et al.* (1989) pointed out that the toxicity of metals is related to the forms in which they exist in the aqueous phase. This is because the interaction of metals with intracellular compartments is highly dependent on chemical speciation. Some species may be able to bind chemically with extracellular proteins and other biological molecules, some may adsorb onto cell walls, and others may diffuse through cell membranes. Consequently, toxicity is more related to the concentrations of metals in a particular species, than to the total concentrations. Geochemical modeling

can be used to calculate the equilibrium species distribution for measured total metal concentrations. Morrison *et al.* (1989) also pointed out that the conclusions about toxic species in the literature are based on calculated equilibrium speciation distributions. Therefore, it is the relevant metal species, not the total concentration, that should be used in risk assessment.

Examples showing that metal speciation is important to metal toxicity include arsenic, copper, selenium, and chromium. While ionic copper (Cu^{2+}) and $CuCl_2^\circ$ are highly toxic, $CuCO_3^\circ$ and Cu-EDTA have low toxicity (Morrison *et al.*, 1989). Toxicity tests show that As(III) is about 50 times more toxic than As(VI). Trivalent chromium is much less toxic than hexavalent chromium, probably because Cr(VI) is much smaller and the chemical structure of chromate is similar to sulfate. A special channel already exists in biomembranes for sulfate transport. While modeling metal speciation is not always possible, and redox equilibrium is not achieved in all natural waters, geochemical modeling of equilibrium species distribution remains one of the methods of discerning metal speciation.

6.4 Interpretations of Column Experiments

Li *et al.* (1996) reported the use of speciation–solubility modeling to interpret the effluent chemistry in column experiments. Noranda Mining and Exploration, Inc. was in the early stage of opening an open pit copper mine at Mines Gaspé in eastern Quebec, Canada. Approximately 20 million tons of oxide ore were to be dissolved with sulfuric acid using a heap leaching operation. After the conclusion of the heap leach operation, the leachate from the spent heap, as a result of rainfall percolation, must meet Canadian government discharge requirements (<0.5 mg L^{-1} for Cu). One decommission option was to rinse the spent heap with clean water and neutralize the acid leachate with limestone or lime.

A large, "pilot scale" column measuring 671 cm in height and 66 cm in diameter was used to study this decommissioning option. Broken but uncrushed ores of about 6 inch size were placed in a column, and rinsing studies commenced after the completion of the copper extraction experiments. Clean water was fed into the top of the column, and leachate was collected weekly at the bottom of the Gaspé Large Column 2.

Figures 6.12, 6.13, and 6.14 show the breakthrough curves for *p*H and major cations and anions from Gaspé Large Column 2. Rinsing volumes were normalized by dividing the total cumulative volumes of water passed through the column by the dry ore weight in that column. Figures 6.15 and 6.16 show the Saturation Indices (SI) calculated from MINTEQA2 using measured *p*H and ion concentrations.

The authors concluded that the leachate reached equilibrium with silica and gypsum because the SI values of these two minerals are constant and close to zero despite the orders of magnitude of concentration differences in sulfate. Solubility control by gypsum also explains the calcium concentration increase at the early washing stage. Calcium concentrations were depressed at first because of the high sulfate concentrations. With the sharp decrease of sulfate concentrations, calcium concentrations increased in response to the decrease in sulfate in the solution.

The solubility control of iron concentrations is evident by the constant SI of goethite

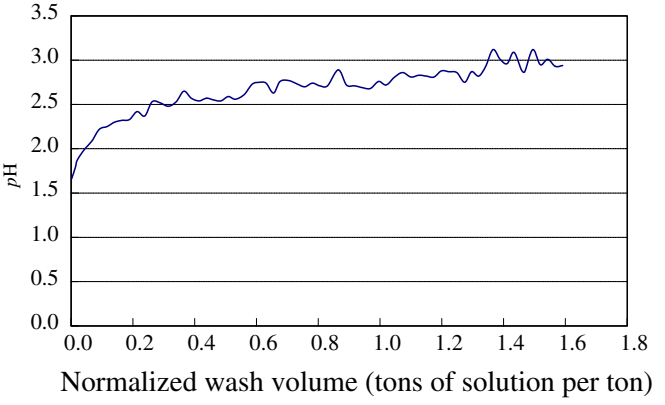

Figure 6.12. *p*H responses to rinsing in Gaspé Large Column 2.

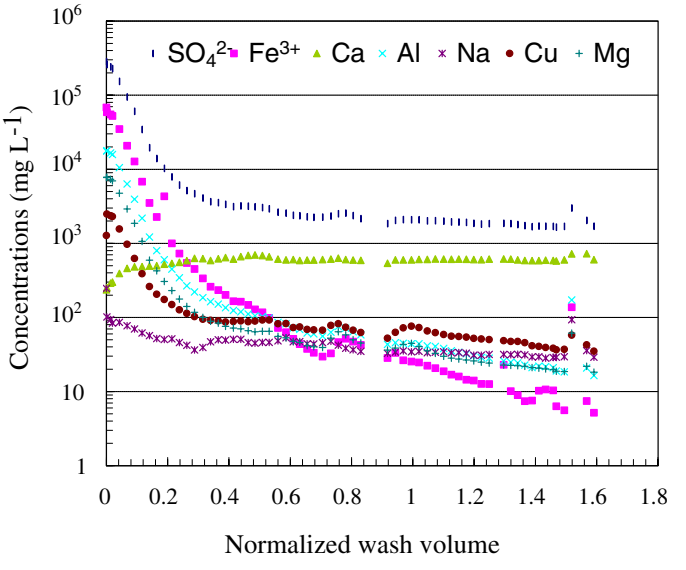

Figure 6.13. Ion concentrations of leachate in Gaspé Large Column 2.

https://doi.org/10.1017/CBO9780511606274.007 Published online by Cambridge University Press

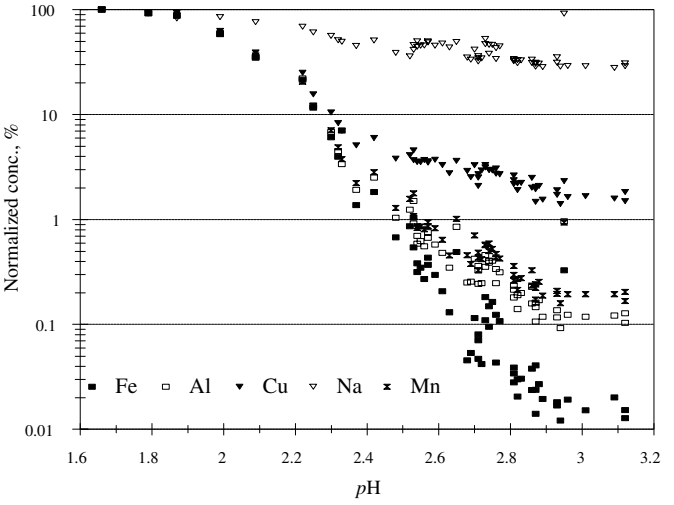

Figure 6.14. Decrease of normalized concentrations as a function of *p*H.

in leachate with varying Fe^{3+} concentrations. Li *et al.* believe that an amorphous iron hydroxide such as ferrihydrite controls the iron solubility. In fact, we see a *p*H buffer effect by $Fe(OH)_3$, similar to the uranium mill tailings site discussed in §6.2. Here, the *p*H buffer occurs at about 0.25 wash volume or a *p*H of about 2.7. We also observe from Figure 6.14 that Fe^{3+} concentrations decrease by three orders of magnitude with an increase of one *p*H unit.

The interpretation by Li *et al.* (1996) was that Al was controlled by $Al(OH)SO_4$ solubility at low *p*H but that this phase was depleted as the washing proceeded. The authors also interpreted the wide range of SI values for jarosites to be a result of the absence of jarosite in the column.

From these column experiments, the authors projected that six wash volumes were needed to rinse the spent heap to meet the government discharge standards. They concluded that relying on rainfall rinsing would take 338 years, but spraying with artificial precipitation using the heap leach irrigation system would be more economical. They estimated that it would cost $5.2 million (Canadian) for this decommission option. Presumably, results from this work were also used in the mining permit application as part of the reclamation plan.

It should be noted that the leachate from the column experiments contains hundreds of thousands of milligrams per liter of dissolved solids, resulting in high ionic strength for the solutions. MINTEQA2 uses the Davies equation and can only accurately simulate solutions with an ionic strength of approximately $\leq 0.2\,m$ (§3.4.2). Therefore, the calculated SI values discussed above bear the errors associated with activity coefficients. It would therefore be useful to recalculate the results of at least one experiment using Pitzer activity coefficients (p. 41), to see if the errors are significant.

Besides geochemistry, transport processes also exert significant controls on effluent concentrations. The dual porosity model (Decker, 1996; Dixon *et al.*, 1993) for

https://doi.org/10.1017/CBO9780511606274.007 Published online by Cambridge University Press

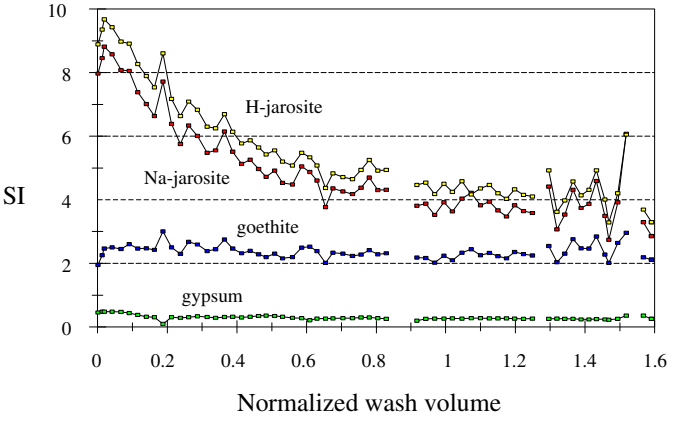

Figure 6.15. Saturation Indices for leachate for Gaspé Large Column 2.

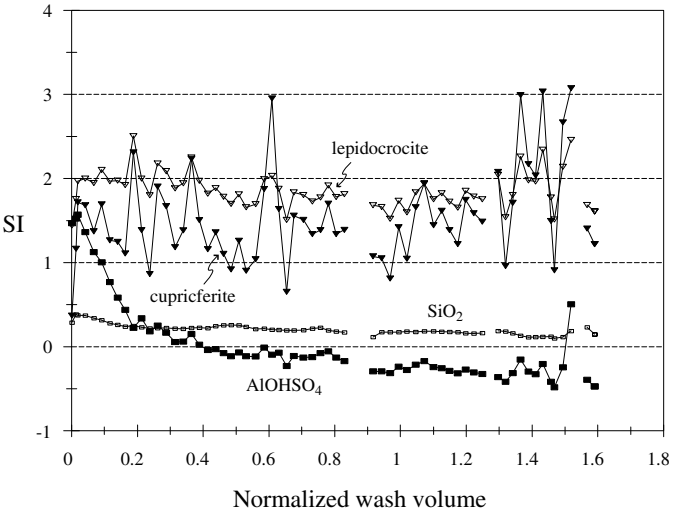

Figure 6.16. Saturation Indices for leachate for Gaspé Large Column 2.

https://doi.org/10.1017/CBO9780511606274.007 Published online by Cambridge University Press

columns packed with spent heap consider macropores where fluid flows preferably and microporosity where fluid flow is stagnant. During initial washing, the leachate residues in the spent heap are displaced by advective transport. Then, the concentrations in the effluent are controlled by matrix diffusion. In reality, reaction kinetics may also come into play in the fast flow and stagnant regions. Speciation and solubility calculations only concern the "state variable", not the quantity of mass or the transport processes. However, they serve as necessary building blocks for an eventual quantitative model.

A similar modeling study was conducted by Stollenwerk (1994) to interpret a column experiment on the acidic water and alluvium sediments interactions for Miami Wash and Pinal Creek, Arizona. He used MINTEQA2 to simulate the equilibrium states in column effluents.

https://doi.org/10.1017/CBO9780511606274.007 Published online by Cambridge University Press